EUROPEAN ORGANIZATION FOR NUCLEAR RESEARCH (CERN)

CERN-EP-2022-268
2022/12/23

CMS-EXO-21-009

Search for new physics in the τ lepton plus missing transverse momentum final state in proton-proton collisions at $\sqrt{s} = 13\,\text{TeV}$

The CMS Collaboration

Abstract

A search for physics beyond the standard model (SM) in the final state with a hadronically decaying tau lepton and a neutrino is presented. This analysis is based on data recorded by the CMS experiment from proton-proton collisions at a center-of-mass energy of 13 TeV at the LHC, corresponding to a total integrated luminosity of $138\,\text{fb}^{-1}$. The transverse mass spectrum is analyzed for the presence of new physics. No significant deviation from the SM prediction is observed. Limits are set on the production cross section of a W′ boson decaying into a tau lepton and a neutrino. Lower limits are set on the mass of the sequential SM-like heavy charged vector boson and the mass of a quantum black hole. Upper limits are placed on the couplings of a new boson to the SM fermions. Constraints are put on a nonuniversal gauge interaction model and an effective field theory model. For the first time, upper limits on the cross section of *t*-channel leptoquark (LQ) exchange are presented. These limits are translated into exclusion limits on the LQ mass and on its coupling in the *t*-channel. The sensitivity of this analysis extends into the parameter space of LQ models that attempt to explain the anomalies observed in B meson decays. The limits presented for the various interpretations are the most stringent to date. Additionally, a model-independent limit is provided.

Submitted to the Journal of High Energy Physics

1 Introduction

A search for new phenomena is conducted in the final state with a high transverse-momentum (p_T) tau lepton (τ) and large missing transverse momentum. This search uses proton-proton (pp) collision data at $\sqrt{s} = 13\,\text{TeV}$ recorded by the CMS experiment at the CERN LHC in 2016–2018, corresponding to an integrated luminosity of $138\,\text{fb}^{-1}$.

The existence of new physics phenomena in the high-m_T region of the τ plus neutrino (ν) final state is predicted by several theoretical models that extend the standard model (SM) of particle physics. These models explore several open issues in modern particle physics. Among them is the large relative difference between the energy scale of electroweak symmetry breaking and that of gravity. This large discrepancy is often referred to as the hierarchy problem [1, 2]. Models attempt to solve the hierarchy problem by extending the gauge group in a way similar to that in left-right symmetric models.

Due to its short lifetime, the τ lepton itself is not detected directly, but via its decay products. The hadronic decays of the τ lepton constitute about 2/3 of all its decays. The hadronic decay products, τ_h, of the tau lepton are distinctive because they result in jets with a lower charged-hadron multiplicity compared to the jets originating from the hadronization of partons produced in the hard scattering process. The selection of the hadronic τ decay mode also allows for discrimination against the leptonic τ decays, which cannot be distinguished from prompt decays to light leptons, such as those examined in the most recent searches by the ATLAS and CMS Collaborations for W′ in the final states with an electron or muon plus a neutrino [3, 4].

The transverse mass, m_T, of the τ-p_T^{miss} system is the primary discriminating variable in this analysis. It is defined as

$$m_T = \sqrt{2 p_T^{\tau_h} p_T^{\text{miss}} [1 - \cos \Delta\phi(\vec{p}_T^{\,\tau_h}, \vec{p}_T^{\,\text{miss}})]}, \tag{1}$$

where $p_T^{\tau_h}$ is the magnitude of the transverse momentum of the reconstructed τ_h candidate, $\vec{p}_T^{\,\text{miss}}$ is the vector of transverse momentum misbalance in the event, p_T^{miss} is its magnitude, and $\Delta\phi(\vec{p}_T^{\,\tau_h}, \vec{p}_T^{\,\text{miss}})$ is the azimuthal opening angle between the directions of $\vec{p}_T^{\,\text{miss}}$ and the tau lepton. We perform the search in a kinematic region where the $\vec{p}_T^{\,\tau_h}$ and the $\vec{p}_T^{\,\text{miss}}$ are approximately balanced and back-to-back in the azimuthal plane.

A new charged gauge boson (W′) is one possible signature of the sequential SM (SSM) [5]. In this model, the W′ boson couplings to fermions are similar to those of the SM W, while the additional decay mode of the W′ boson to top and bottom quarks is allowed for a sufficiently high boson mass. Searches for an SSM-like W′ boson decaying to the $\tau + \nu_\tau$ final state have previously been reported by the CMS Collaboration at 8 TeV [6] and 13 TeV [7], as well as by the ATLAS Collaboration at 13 TeV [8]. These searches by the ATLAS and CMS experiments excluded W′ bosons with masses up to 3.7 TeV and 4.0 TeV, respectively. The W′ coupling strengths may differ from that of the SM W or the SSM W′ bosons. Therefore, we also consider the case where the ratio $g_{W'}/g_W$ of the W′ boson coupling strength to that of the SM W boson is not unity. The nonuniversal gauge interaction model (NUGIM) predicts an enhanced branching fraction for decays into third-generation fermions. We also place upper exclusion limits on the ratio of the W′ boson coupling strength to the W boson coupling strength and on the NUGIM.

Some models of leptoquarks (LQs) are particularly interesting in light of the significant deviations from the SM prediction in measurements in the flavor sector of $B \to D^*$ transitions, by the BaBar [9, 10], Belle [11–14], and LHCb [15–17] Collaborations. Deviations have also been found

in recent measurements of $B \to K^*$ transitions that have been performed by the LHCb Collaboration [18–21]. The values presently measured by LHCb are in tension with the SM prediction by between 1.4 and 3.1 standard deviations. The postulate of TeV-scale LQs with dominant couplings to third-generation fermions is among the favored theoretical attempts to explain these anomalies [22–44]. While numerous searches for single or pair production of LQs with dominant couplings to third-generation fermions at the LHC have yielded null results [45–55], the first search for LQ t-channel exchange in the $\tau + \nu$ final state is presented here.

If the excess seen in the $B \to D_s$ transitions is indeed due to new physics, the mass scale of its manifestation is expected to be at the TeV scale or not far beyond [56]. To provide a different test for the presence of new physics, a description based on an effective field theory (EFT) [57] with different types of coupling coefficients referred to as Wilson coefficients is also considered.

In models with extra spatial dimensions, the hierarchy problem can be solved by lowering the fundamental Planck scale to the TeV range, which implies that gravity is strongly coupled at the LHC energies. In this case, the production of microscopic black holes may be possible at the LHC [58, 59]. In some models [60], these black holes would decay nonthermally into pairs of particles. Such black holes are often called quantum black holes (QBHs).

The shape of the m_T distribution is interpreted using a binned-likelihood method for the SSM, QBH, and EFT descriptions. We set upper exclusion limits on the cross section times branching fraction ($\sigma\mathcal{B}$) for the SSM description as a function of the mass of the new resonance ($m_{W'}$) and for the QBH model as a function of the mass scale of the QBH (m_{QBH}). In the case of the EFT description, upper exclusion limits are placed on the Wilson coefficients. Additionally, a model independent limit setting method is considered and discussed.

The paper is structured as follows: the CMS detector is briefly described in Section 2. The models examined in this analysis are outlined in Section 3. The data and simulated samples used are presented in Section 4, while Section 5 describes the event reconstruction and the kinematic selection of the signal region. The specific determination of the background from misidentified τ leptons is described in Section 6. Section 7 reviews the most important sources of systematic uncertainties and their impact on the measurements. The results and achieved sensitivity for all the models are detailed in Section 8 and summarized in Section 9. The results are also documented in HEPData [61].

2 The CMS detector

The central feature of the CMS apparatus is a superconducting solenoid of 6 m internal diameter, providing a magnetic field of 3.8 T. Within the solenoid volume are a silicon pixel and silicon strip tracker, measuring the charged particle trajectories inside a pseudorapidity (η) acceptance of $|\eta| < 2.5$. Also within the solenoid volume are a lead tungstate crystal electromagnetic calorimeter (ECAL), and a brass and scintillator hadron calorimeter (HCAL). Each subdetector is composed of a barrel and two endcap sections. Forward calorimeters extend the pseudorapidity coverage provided by the barrel and endcap detectors. Muons are detected in gas-ionization detectors embedded in the steel flux-return yoke outside the solenoid.

Events of interest are selected using a two-tiered trigger system. The first level, composed of custom hardware processors, uses information from the calorimeters and muon detectors to select events at a rate of around 100 kHz within a fixed latency of about 4 μs [62]. The second level, known as the high-level trigger, consists of a farm of processors running a version of the full event reconstruction software optimised for fast processing, and reduces the event rate to

around 1 kHz before data storage [63].

A more detailed description of the CMS detector, together with a definition of the coordinate system used and the relevant kinematic variables, can be found in Ref. [64].

3 Physics models

This section describes the different signal models used in this paper. All of these models predict physics beyond the SM that would be detectable in a final state with a τ lepton and missing transverse momentum.

3.1 The SSM heavy charged vector boson

In the SSM, the W′ boson is a heavy analogue of the W boson. The experimental signature would be a resonance with fermionic decay modes and branching fractions similar to those of the SM W boson. For W′ boson masses larger than 180 GeV the additional $\mathrm{W}' \to \mathrm{tb}$ decay mode becomes relevant. If this decay is considered, the branching fraction for the $\mathrm{W}' \to \tau\nu$ decay in the SSM is 8.5% [5]. Under these assumptions, the relative decay width of a 1 TeV W′ boson is $\Gamma/M \approx 3.3\%$. Decays to W and Z bosons are assumed to be suppressed in the SSM. No interference between the production of the new particle and the production of the SM W boson is assumed. This is justified by the fact that the subsequent hadronic decay of the τ lepton leads to two neutrinos being present in the final state, significantly lowering the effect an interference of W′ and W might have. The leading order (LO) Feynman diagram for this specific process is given in Fig. 1.

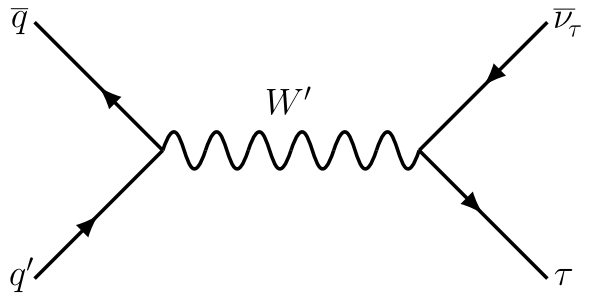

Figure 1: Leading order Feynman diagram for the production and decay of a new heavy charged vector boson, W′, decaying to $\tau\overline{\nu}_\tau$.

3.2 Varying coupling strength

In the SSM, the W′ boson coupling strength, $g_{\mathrm{W}'}$ is assumed to be identical to the SM W boson coupling, g_{W}. However, we also consider cases where $g_{\mathrm{W}'} \neq g_{\mathrm{W}}$. Because the W′ boson width and cross section also depend on $g_{\mathrm{W}'}$, we can interpret the kinematic distributions with respect to W′ particles as described by various coupling values. The W′ boson coupling strength is given in terms of the SM weak coupling strength $g_{\mathrm{W}} = e/\sin^2\theta_{\mathrm{W}} \approx 0.65$, where e is the electron charge and θ_{W} is the weak mixing angle.

3.3 Nonuniversal gauge interaction model

Models with nonuniversal couplings predict an enhanced branching fraction for decays into the third generation of SM fermions. These models could offer an explanation as to why the mass of the top quark is so large [65–67]. The NUGIM exhibits an $SU(2)_\ell \times SU(2)_\mathrm{h} \times U(1)$ symmetry. The symmetry groups $SU(2)_\ell$ and $SU(2)_\mathrm{h}$ govern the couplings of the gauge bosons to

the light fermions of the first two generations and to the heavy fermions of the third generation, respectively. Models of this type are often called G(221) models. The weak SM $SU(2)_{\mathrm{L}}$ group is a low-energy limit of two gauge groups: $SU(2)_{\ell}$ and $SU(2)_{\mathrm{h}}$.

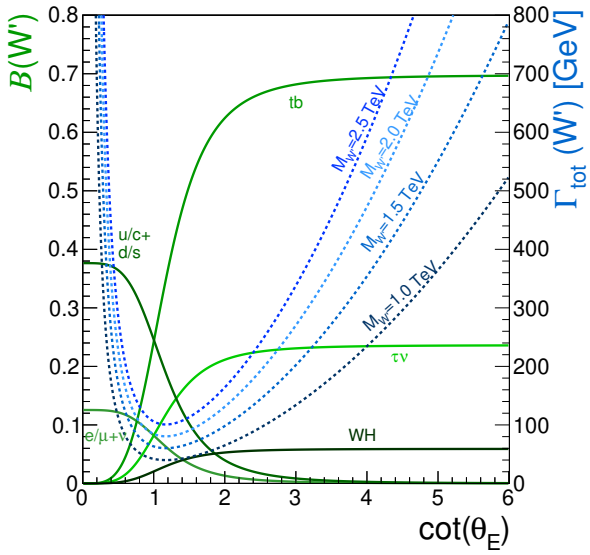

Figure 2: Branching fractions $\mathcal{B}(\mathrm{W}')$ as function of the mixing angle $\cot\theta_{\mathrm{E}}$ (solid lines), for W′ boson decays in the NUGIM G(221) framework, as calculated in Refs. [65–67]. The total decay width Γ_{tot} (dotted lines) can also be determined as a function of the mixing angle. When re-scaled to accommodate the W H decay channel, the values associated with $\cot\theta_{\mathrm{E}} = 1$ correspond to those in the SSM.

These groups combine via a mixing angle θ_{E}, resulting in an SM-like $SU(2)_{\mathrm{L}}$ group and an additional extended group $SU(2)_{\mathrm{E}}$. This extended group gives rise to additional heavy gauge bosons such as the W′ boson. The mixing angle directly affects the cross section and decay width of such particles, as shown in Fig. 2. As can be seen, for $\cot\theta_{\mathrm{E}} = 1$ the branching fractions are equal for all lepton flavors, which would correspond to an SSM-like feature. When re-scaled to accommodate the W H decay channel, the values associated with $\cot\theta_{\mathrm{E}} = 1$ correspond to those in the SSM. For values larger than one, the decay to τ leptons becomes dominant. The mixing angle changes the production cross section and the branching fractions of the W′ boson. In the NUGIM, decays to W and Z bosons are negligible by construction, while decays to W H bosons typically have a branching fraction $<6\%$.

In the NUGIM G(221), neglecting the small contribution from the W H decay, the ratio of the couplings, $g_{\mathrm{W}'}/g_{\mathrm{W}}$, is related to the parameter $\cot\theta_{\mathrm{E}}$ by the following equation [67]:

$$\Gamma_{\mathrm{W}'} = \Gamma^{\mathrm{SSM}}_{\mathrm{W}'} \frac{(4+\frac{1}{4})\cot^2\theta_{\mathrm{E}} + 8\tan^2\theta_{\mathrm{E}}}{12+\frac{1}{4}} = \Gamma^{\mathrm{SSM}}_{\mathrm{W}'} \left(\frac{g_{\mathrm{W}'}}{g_{\mathrm{W}}}\right)^2 . \tag{2}$$

Because of this functional relationship, a reinterpretation of the limits on the coupling strength yields limits on the parameters of NUGIM G(221). Therefore, the SSM W′ signal samples mentioned in Section 4.1 can be used to probe this model. The product of the cross section and branching fraction, $\sigma\mathcal{B}$, scales with $\Gamma_{\mathrm{SSM}}/\Gamma_{\mathrm{NUGIM}}$.

3.4 Quantum black holes

Theories that invoke extra spatial dimensions often permit a fundamental Planck scale in the TeV region. Such theories also provide the possibility of producing microscopic black holes at

LHC energies [58, 59]. In models with QBHs [60], the regime at which gravity becomes strongly coupled to SM particles causes the theory to become non-perturbative. This creates unavoidable limitations. When working in these regimes, usage of the model and its predictions should be viewed as a dimensional analysis in which some extrapolations from the classical domain carry over to the QBHs. In contrast to semiclassical thermal black holes that can decay to high-multiplicity final states, QBHs are nonthermal objects, expected to decay predominantly to pairs of particles. Despite not having a complete theory of quantum gravity, it is still possible to gain insight into the signatures of QBHs at the LHC based on some fundamental principles and a few assumptions. The cross section for QBH production depends on the threshold mass, m_{th}, in n additional spatial dimensions. The $n > 1$ cases correspond to the Arkani-Hamed–Dimopoulos–Dvali model [68]. In this search the number of extra dimensions is assumed to be n=4. The m_{th} distribution of the QBH signal is characterized by a sharp edge at the threshold of QBH production, followed by a monotonic decrease at larger masses.

3.5 Leptoquarks

Leptoquarks are hypothetical new scalar or vector bosons carrying both baryon and lepton numbers and an electric charge in multiples of $(1/3)\,e$. The postulation of TeV-scale LQs with dominant couplings to third-generation fermions is a popular theoretical explanation of the observed anomalies in the ratio of branching fractions of B meson decays

$$R_{K^*} = \frac{\mathcal{B}(B \to K^* \mu\mu)}{\mathcal{B}(B \to K^* ee)} \tag{3}$$

and the ratio of the widths of semileptonic B meson decays

$$R_{D^*} = \frac{\Gamma(B \to D^* \tau\nu)}{\Gamma(B \to D^* \ell\nu)} \tag{4}$$

where ℓ = e or μ.

Under the assumption that their couplings to the SM fermions are renormalizable and gauge invariant, the possible quantum numbers of LQs are restricted to those given in the Buchmüller–Rückl–Wyler model [69].

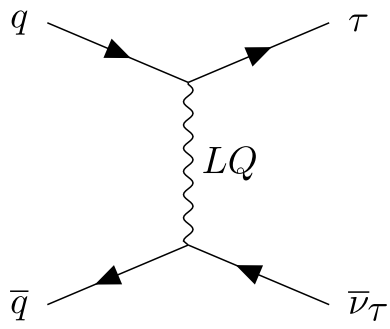

Figure 3: Leading order Feynman diagram of the process $pp \to \tau\overline{\nu}_\tau$ mediated via a leptoquark in the t-channel.

At the LHC, the final state with one τ lepton and p_T^{miss} can be produced by an LQ appearing as a t-channel propagator, leading to a nonresonant enhancement of events with large values of m_T. The LO Feynman diagram of this process is shown in Fig. 3. The cross section of this process depends on the mass of the LQ (m_{LQ}) and its coupling g_U to SM fermions. While the

dependence of the cross section on m_{LQ} is weaker for a LQ in the t-channel compared to single or pair LQ production, it scales with g_{U}^4 at LO.

In models addressing the tension in the flavor sector, LQs are often predicted to have flavor-nonuniversal couplings to left- (LH) and right-handed (RH) fermions, effectively modifying the LQ coupling to LH and RH SM fermions to be $g_{\mathrm{U}}\beta_{\mathrm{L}}^{ij}$ and $g_{\mathrm{U}}\beta_{\mathrm{R}}^{ij}$, respectively. Here, β_{L}^{ij} and β_{R}^{ij} are complex 3×3 matrices with i and j denoting the down-type quarks and leptons, respectively. The normalization of g_{U} is chosen such that $\beta_{\mathrm{L}}^{\mathrm{b}\tau} = 1$.

Three coupling benchmark scenarios are considered in this analysis, two of which have been proposed in Ref. [44]. The first two scenarios are the result of a fit of the parameters of a $U(1)$ vector LQ of charge $(-1/3)e$ to explain the flavor anomalies in R_{K^*} (Eq. (3)) and R_{D^*} (Eq. (4)) and other related observables. The first benchmark scenario considers only couplings to LH SM fermions (i.e., $\beta_{\mathrm{R}}^{ij} = 0$) and is referred to as "best fit LH" in the following. The second benchmark, referred to as "best fit LH+RH", additionally considers $\left|\beta_{\mathrm{R}}^{\mathrm{b}\tau}\right| = 1$ with all other $\beta_{\mathrm{R}}^{ij} = 0$. In the third "democratic" benchmark, equal couplings only to LH fermions are assumed, i.e. $\left|\beta_{\mathrm{L}}^{ij}\right| = 1$ and $\beta_{\mathrm{R}}^{ij} = 0$ for all i and j.

3.6 Effective field theory description

As mentioned above, the ratio in Eq. (4) appears to be enhanced with respect to the SM expectation by approximately 30%. If this enhancement originates from new physics, the corresponding mass scale of this physics is expected to be at, or near, the TeV scale [56]. The aim of this model is to search for any prescription that is able to address the R_{D^*} anomalies with new heavy mediators. It uses a low-energy EFT of new physics in semi-leptonic $(\mathrm{b} \to \ell\nu\mathrm{c})$ transitions and translates this into a predictive theory at the TeV scale [57]. This EFT model introduces three Wilson coefficients — one for the LH vector coupling $\epsilon_{\mathrm{L}}^{\mathrm{cb}}$, one for tensor like coupling $\epsilon_{\mathrm{T}}^{\mathrm{cb}}$, and one for scalar-tensor like coupling $\epsilon_{\mathrm{S_L}}^{\mathrm{cb}}$.

4 Data and simulated events

4.1 Data

In this search, we analyze a data set from pp collisions at a center-of-mass energy of 13 TeV that was recorded by the CMS experiment in 2016–2018 and corresponds to an integrated luminosity of 138 fb^{-1}. Events were selected with an isolated single τ trigger with $|\eta| < 2.1$ and with p_{T} thresholds of 120 GeV in 2016 and 180 GeV in 2017–2018. The τ trigger is complemented with a $p_{\mathrm{T}}^{\mathrm{miss}}$ trigger with a 120 GeV threshold. The trigger efficiency for simulated signal events that pass the offline selection criteria is about 95%. The efficiency of the τ trigger estimated using Monte Carlo simulations typically differs from that measured with data by approximately 10% (depending on the particular p_{T} bin) across all data-taking years. The estimated $p_{\mathrm{T}}^{\mathrm{miss}}$ trigger efficiency from simulation is only 1–4% above or below data depending on the $p_{\mathrm{T}}^{\mathrm{miss}}$ bin. We correct these differences in trigger efficiency between simulation and data using efficiency correction factors, which are henceforth referred to as scale factors. The scale factors range from 0.88–0.99 (0.87–1.08) for the 2016 (2017–2018) datasets.

4.2 Event simulation

Generated events are processed through a simulation of the detector geometry and response using GEANT4 [70]. The same reconstruction software is applied to both data and simulated

events. Backgrounds are simulated using an expected distribution of the number of additional pp interactions within the same or nearby bunch crossings (pileup). All simulated backgrounds are reweighted such that the distribution of the number of collisions per bunch crossing matches the data, with an average of approximately 23 (32) interactions per bunch crossing [71–73] in 2016 (2017–2018). Unless otherwise noted, simulated samples use the underlying event tune CUETP8M1 [74] in 2016 and the CP5 tune [75] in 2017–2018.

4.2.1 Signal simulation

The SSM W′ boson signal samples ($q'\bar{q} \rightarrow W'$) are generated at LO using PYTHIA 8.2.05 [76] for each data-taking year, and employing the NNPDF2.3 [77] (NNPDF3.1 [78]) parton distribution function (PDF) set for the 2016 (2017–2018) configurations. These samples are generated for mass points ranging from 0.6 to 6.0 TeV. To interpret the results in terms of the coupling ratio of the SSM W′ boson and the SM W boson, signal samples are simulated at LO using MADGRAPH5_aMC@NLO version 2.6.5 [79, 80] for different coupling ratios $g_{W'}/g_W$ for coupling ratio values of [0.001, 0.01, 0.1, 1.0, 2.0, 3.0, 5.0], for all mass points.

Signal samples of LQ t-channel exchange at LO using MADGRAPH5_aMC@NLO are generated for LQ masses between 0.1 and 10 TeV neglecting interference with SM processes. Interference is expected to be negligible in the phase space sensitive to this signal [81]. The parton shower, hadronization, and underlying event are modelled with PYTHIA 8. The underlying event tune CP2 [75] is used for 2017 and 2018. The NNPDF2.3 and NNPDF3.1 PDF sets are used for 2016 and 2017–2018, respectively.

The QBH signal samples are generated with the QBH 3.0 generator [82]. We consider the $q'\bar{q}$ production of a singly positively charged QBH with its subsequent decay to a τ lepton and a neutrino. Signal samples with minimum threshold masses from 400 to 11000 GeV are employed. The CTEQ6L1 PDF set [83], which is the recommended PDF for QBHs, is used. The definition of the Q scale for PDFs is taken to be the inverse of the gravitational radius.

Signal samples for the EFT model are generated using MADGRAPH5_aMC@NLO at LO, while simulation of the hadronization and τ lepton decay is performed using PYTHIA 8. The signal samples are generated with MADGRAPH5_aMC@NLO using the values 0.3, 1.0, and 0.3 for the Wilson coefficients (ϵ_L^{cb}, ϵ_T^{cb}, $\epsilon_{S_L}^{cb}$), respectively, which are obtained by fitting them to the current values of R_{D^*} [84]. The event content of these signal samples can be rescaled to cover a wider range of coupling values. The CP2 tune is used in conjunction with NNPDF3.1 PDF set for generation of signal samples.

4.2.2 Simulation of the background

Background processes for this analysis include off-shell SM W production, processes coming from the decay of top quarks ($t\bar{t}$), the Drell–Yan (DY) process, and diboson (ZZ, WW, WZ) processes. These samples are produced with PYTHIA 8 (for SM W), MADGRAPH5_aMC@NLO (for DY, ZZ, and WZ), and POWHEG 2.0 [85–87] (for $t\bar{t}$ and WW). Backgrounds are simulated using the NNPDF3.0 (NNPDF3.1) NNLO [88] PDF set for 2016 (2017–2018).

The SM background expected in this search consists of two different types of events: those where the τ candidate originates from a gluon- or quark-initiated jet, and others where the τ originates from a genuine τ lepton decay. The former is derived from data, while the latter is estimated using simulation.

The dominant irreducible background for this analysis comes from SM $W \rightarrow \tau\nu$ production. This background is generated at LO precision in quantum chromodynamics (QCD) with

PYTHIA 8 for high-mass off-shell production. On-shell production is generated at LO precision in QCD with MADGRAPH5_aMC@NLO, and the simulated jets are matched to the matrix element and parton shower produced by PYTHIA using MLM [79] merging. The differential cross section is reweighted as a function of the invariant mass of the SM W boson, incorporating next-to-LO (NLO) electroweak (EW) and next-to-NLO (NNLO) QCD corrections. The EW and QCD corrections can be combined by two different mathematical approaches: additive and multiplicative [89]. These approaches differ by approximately 5%. The applied correction factor uses the recommended additive approach [90], which is parametrized using a fit of a fourth order polynomial function. Differences between this approach and the multiplicative approach are taken as a systematic uncertainty. The calculation uses the FEWZ 3.1 and MCSANC 1.01 [91, 92] generators for the QCD and EW corrections, respectively.

5 Event selection and particle identification

The particle-flow algorithm [93] aims to reconstruct and identify each individual particle in an event, with an optimized combination of information from the various subsystems of the CMS detector. We obtain the photon energy from the ECAL measurement. Electron energy is determined from a combination of the electron momentum at the primary interaction vertex as determined by the tracker, the energy of the corresponding ECAL cluster, and the energy sum from all bremsstrahlung photons spatially compatible with originating from the electron track. Muon energy is obtained from the curvature of the corresponding track. Charged-hadron energy is determined from a combination of the momentum of the hadron measured in the tracker and matching ECAL and HCAL energy deposits, corrected for the response function of the calorimeters to hadronic showers. Neutral-hadron energy is obtained from the energy deposits in the ECAL and HCAL corrected in a similar way to that of the charged hadrons.

For each event, hadronic jets are clustered from these reconstructed particles using the infrared- and collinear-safe anti-k_{T} algorithm [94] in the FASTJET software package [95] with a distance parameter of 0.4. The jet momentum is determined as the vectorial momentum sum of each particle contained within the jet. From simulation, we find the jet momentum to be, on average, within 5–10% of the true momentum over the entire p_{T} spectrum and detector acceptance. Pileup can contribute additional tracks and calorimetric energy depositions to the jet momentum. To mitigate this effect, we discard charged particles identified to be originating from pileup vertices and apply an offset to correct for remaining contributions. Jet energy corrections are derived from simulation to bring the measured response of jets to be similar to that of particle-level jets, on average. In situ measurements of the momentum balance in dijet, photon+jet, Z +jet, and multijet events are used to account for any residual differences in the jet energy scale between data and simulation [96]. The jet energy resolution, obtained from a dijet balance technique, is found to be 15–20% at 30 GeV, 10% at 100 GeV, and 5% at 1 TeV [96]. We apply additional selection criteria to each jet to remove jets potentially dominated by anomalous contributions from various subdetector components or reconstruction failures [97].

The missing transverse momentum vector $\vec{p}_{\mathrm{T}}^{\,\mathrm{miss}}$ is computed as the negative vector p_{T} sum of all of the particle-flow candidates in an event, and its magnitude is denoted as $p_{\mathrm{T}}^{\mathrm{miss}}$. The $\vec{p}_{\mathrm{T}}^{\,\mathrm{miss}}$ is modified to account for corrections to the energy scale of the reconstructed jets in the event [97]. Anomalous high-$p_{\mathrm{T}}^{\mathrm{miss}}$ events can occur due to a variety of reconstruction failures, detector malfunctions, or non-collision backgrounds. We reject such events by using event filters designed to identify more than 85% of the spurious high-$p_{\mathrm{T}}^{\mathrm{miss}}$ events, with a mistagging rate less than 0.1% [97].

The τ_{h} candidates are reconstructed using the Hadron-plus-Strip (HPS) algorithm [98] starting

from a jet. To reconstruct the τ_h decay mode and its four momentum, we consider all particles in an η–ϕ cone of radius $\Delta R = 0.5$ around the jet axis. This candidate is subsequently compared with quark or gluon-initiated jets, electrons, and muons. We apply corrections for the small differences in the τ_h energy between simulation and data.

To distinguish between τ_h candidates originating from genuine τ leptons and other objects, we use the DEEPTAU identification [99] . This identification method consists of a convolutional deep neural network that uses machine learning techniques and image recognition methods in order to discriminate genuine τ_h candidates from light leptons and jets. It combines high-level variables, such as the τ lepton isolation, with low-level variables such as specific energy deposits in CMS subdetectors. This method has been shown to provide excellent discrimination against these jets, electrons, and muons while retaining a high efficiency for genuine τ leptons. The identification efficiency of genuine τ_h candidates ($p_T > 100$ GeV) provided by the chosen identification method in this analysis is approximately 75%, while the probability of a jet being misidentified as a τ lepton is less than 0.7%. Differences between data and simulation arising from the application of the identification method are corrected for using scale factors. Corrections due to differences in τ identification performance and energy scale measurements are less than 5%.

We select τ_h candidates with a $p_T^{\tau_h} > 130$ (190) GeV for data recorded in 2016 (2017–2018). The τ_h candidate is required to be in the range $|\eta| < 2.1$. Additionally, we require τ_h candidates to pass anti-jet, anti-electron, and anti-muon discriminators of the DEEPTAU algorithm in order to reduce their corresponding misidentification probabilities [99]. The p_T^{miss} associated with these events is required to be at least 200 GeV.

In order to reduce the number of misidentified light leptons and to reduce background, we reject events containing loosely identified electrons [100] or muons [101] with $p_T \approx> 20$ GeV within the detector acceptance. Events containing more than one τ_h candidate fulfilling the identification criteria are also rejected. The τ_h decay products and the neutrino are expected to be back-to-back to each other for all signal processes. The neutrino created during the τ lepton decay is emitted in a similar direction to that of the τ lepton in the laboratory frame and therefore only slightly reduces the overall magnitude of the expected $\vec{p}_T^{miss}$. Thus, we require $0.7 < p_T^{\tau_h}/p_T^{miss} < 1.3$ and $|\Delta\phi(\vec{p}_T^{\tau_h}, \vec{p}_T^{miss})| > 2.4$. The variable used to determine the signal yields for this analysis is the transverse mass, m_T, as shown in Eq. (1).

6 Jet background estimation

We use data to estimate the backgrounds due to jets misidentified as τ_h candidates. In this analysis, this background contribution originates mostly from QCD multijet and Drell–Yan events. The signal-free control region comprises events with one well reconstructed light lepton and a τ_h candidate. These events are selected using single light lepton triggers. The misidentification rate is defined as the number of τ lepton candidates passing the full selection criteria divided by the number of those candidates that do not fulfill the isolation requirement. This rate is calculated as a function of the τ lepton candidate p_T and the number of charged hadrons within the τ lepton candidate isolation cone ($\Delta R = 0.5$). Events where a τ lepton is matched to a generator-level τ lepton in simulation are subtracted from data. The ratio is estimated at approximately 5% for τ lepton decays involving three charged hadrons and up to 30% for τ leptons that decay into one charged hadron. The rate is then applied as an event-weight to signal-like events where a τ lepton candidate does not fulfill the isolation requirement. This application region primarily contains events originating from misidentified jets, with a small

contamination of genuine τ_h candidates. This contamination is subtracted from the application region using input from simulation.

This method is validated by estimating the ratio of simulated events in which jets are misidentified as τ_h candidates, applying it to signal-like events where a τ lepton candidate does not fulfill the isolation requirement, and comparing the results to the background prediction from simulation in the signal region. In order to account for the differences found with this validation, and to cover uncertainties arising from differences in the misidentification rate measurements from the individual sideband regions, corresponding uncertainties are applied.

7 Systematic uncertainties

There are various sources of uncertainties that can affect the normalization or the shape of the m_T distribution. These affect either the signal or the background estimates. We consider three types of systematic uncertainties: normalization, shape-based, and statistical.

The dominant uncertainty that affects the shape of the m_T distribution arises from the PDF sets used in simulating the background processes. We calculate this uncertainty with the PDF4LHC procedure [102], using replicas of the NNPDF3.0 (NNPDF3.1) PDF set for 2016 (2017–2018). This uncertainty grows with increasing m_T and becomes as large as 50% in the highest bin (> 1.8 TeV) of the m_T distribution.

Another source of uncertainty comes from corrections to the measured τ lepton energy scale (1.5–4.0% for $p_T^{\tau_h} > 100$ GeV, depending on the decay mode), τ identification efficiency (up to 5% for 1 TeV τ leptons), and τ trigger scale factors ($\approx 10\%$). Uncertainties coming from shifting the jet energy scale and resolution are propagated to the calculation of $\vec{p}_T^{\,miss}$.

For all backgrounds estimated at NLO, factorization and renormalization scales are each multiplied by three factors (0.5, 1.0, 2.0), with the combination (1.0, 1.0) being the nominal. The largest deviations in the resulting event yield predictions, both up and down from the nominal value, are taken as systematic uncertainty. Variations where one scale is multiplied by 0.5 and the other by 2 are considered unphysical and are not considered.

Events in simulation are reweighted based on pileup differences between measured data and simulation. The total inelastic cross section of 69.2 mb [103] is varied by $\pm 5\%$ and the resulting final m_T distribution is recalculated to estimate the uncertainty.

Uncertainties that affect the normalization of the background modeling arise from the measurement of the integrated luminosity, as well as from uncertainties in the cross sections of specific backgrounds. For the integrated luminosity, we apply an uncertainty of 1.2%/2.3%/2.5% for the year 2016/2017/2018, respectively, which correspond to the combined uncertainty of 1.6% for the full data-taking period. The cross section uncertainties are evaluated as 4% for the diboson background and 2% for the Drell–Yan background. The background from misidentified τ lepton candidates is estimated with a normalization uncertainty of 100%. Additionally, we estimate the systematic uncertainty in the calculated ratio arising from the statistical uncertainties in the control and application regions. For the dominant W boson background, we apply the W boson mass-dependent uncertainties as explained in Section 4.2.2. Uncertainties in the jet background estimation include uncertainties from the misidentification ratio measurement, as well as the statistical uncertainties from both control and application regions of the method. Statistical uncertainties arise from data and from the limited event count in simulated background samples, and are taken into account [104]. These uncertainties are treated as uncorrelated between the bins of the final m_T distribution. The combination of all uncer-

tainties shows an increasing trend with increasing m_{T}. Because the number of total expected background events becomes small, this does not affect the sensitivity by a significant amount for high-mass objects.

All systematic uncertainties are treated as fully correlated across years, except for those where the uncertainty arises from statistically independent sources. The uncertainties of the data-driven background are treated as uncorrelated across years. Correction uncertainties related to τ_{h} and $p_{\mathrm{T}}^{\mathrm{miss}}$ and the luminosity uncertainties are treated as partially correlated since they include some components that are considered correlated between years and some others that are not.

8 Results

Figure 4 displays the distribution for hadronically decaying τ lepton events with missing transverse momentum, for the combined 2016–2018 data set. To illustrate signal distributions for the models described in this analysis, simulated SSM W′ boson samples, as well as simulated QBH and EFT samples are included in the figure. The W′ boson masses, $m_{\mathrm{W}'}$, of 1.0 and 5.0 TeV are used for the SSM samples, a QBH mass, $\mathrm{m}_{\mathrm{QBH}}$, of 5.0 TeV is used for the QBH sample, and a tensor-type EFT sample is used to show the expected effect of the Wilson coefficients on the m_{T} distribution. The main background contribution comes from off-shell W boson production, followed by events with misidentified τ leptons. Backgrounds from misidentified τ leptons are estimated using the data-driven technique described in Sec. 6. Other backgrounds are estimated using simulation. Example signal distributions are normalized to a cross section of 10 fb. The bin width increases with transverse mass.

The data agree with the expected background yields within statistical and systematic uncertainties. No significant deviation from the SM prediction is observed. We calculate limits at 95% confidence level (CL) from the m_{T} distribution using Bayesian methods known to have good frequentist coverage properties [105]. A software framework designed specifically to combine Higgs boson searches [106], based on the ROOSTATS package [107], is used to calculate the limits. For these limit calculations, we use a Bayesian method with a uniform positive prior probability density for the signal cross section. The nuisance parameters connected to shape-based uncertainties are modeled using a template-morphing technique, while those affecting the normalization of the distribution are included using a log-normal prior. To search for resonances in the m_{T} spectrum, a binned maximum likelihood fit is performed.

We calculate upper exclusion limits on $\sigma\mathcal{B}$ for each model described in Section 3. We further translate these into lower exclusion limits on $m_{\mathrm{W}'}$ and m_{QBH} for the SSM W′ and QBH models, respectively. However, for the studies focused on coupling strengths, these are left as upper exclusion limits, unless otherwise specified.

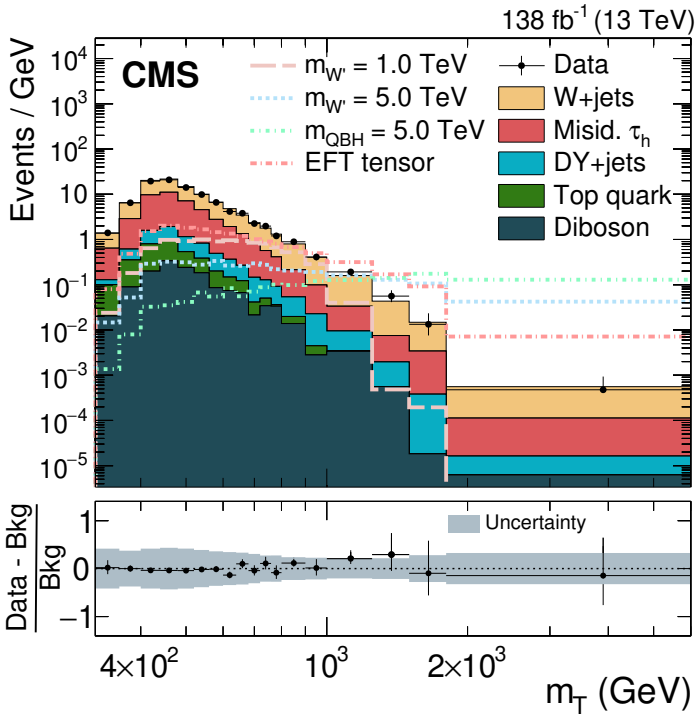

Figure 4: The transverse mass distribution of the $\tau_h + p_T^{miss}$ system observed in the 2016–2018 data (black dots with statistical uncertainty) as well as the expectation from SM processes (stacked histograms). The horizontal lines of the data points reflect the varying bin sizes. Different signal hypotheses normalized to $10\,fb^{-1}$ are illustrated as dashed lines for exemplary SSM W′ boson, QBH, and EFT signal hypotheses. The ratios of the background-subtracted data yield to the expected background yield are presented in the lower panel. The combined statistical and systematic uncertainties in the background are represented by the grey shaded band in the ratio panel.

8.1 Model-independent cross section limit

New physics might produce signal shapes that are different from those expected for any of the above-mentioned signal models. Therefore, a model-independent (MI) cross section limit on $(\sigma\mathcal{B}A\epsilon)_{\mathrm{MI}}$ is provided in Fig. 5. This limit is obtained by calculating a single bin limit, where we integrate from a lower m_{T} threshold to infinity. This procedure results in an exclusion limit with a step-like behavior that originates from the binning of the m_{T} distribution. For the estimation of this exclusion limit, a constant product of acceptance times efficiency of 16% is assumed. This value includes the branching fraction of hadronic τ lepton decays and experimental efficiencies for the signal. An exclusion limit on a specific model calculated using the presented MI limit can be obtained by applying the model-dependent part of $A\epsilon$.

To reflect the effect of the threshold, $m_{\mathrm{T}}^{\mathrm{min}}$ on a new physics signal, we determine a factor $f_{m_{\mathrm{T}}}$ by counting the number of events with $m_{\mathrm{T}} > m_{\mathrm{T}}^{\mathrm{min}}$ and dividing this result by the number of generated events. The reconstruction efficiency is nearly constant over the entire m_{T} range scanned in this analysis; therefore $f_{m_{\mathrm{T}}}$ can be evaluated at the generator level.

A limit on the product of the production cross section and branching fraction $(\sigma\mathcal{B}A\epsilon)_{\mathrm{excl}}$ together with the acceptance A and the efficiency ϵ can be obtained as a function of $m_{\mathrm{T}}^{\mathrm{min}}$ by dividing the excluded cross section of the MI limit $(\sigma\mathcal{B}A\epsilon)_{\mathrm{MI}}$ given in Fig. 5 by the calculated fraction $f_{m_{\mathrm{T}}}(m_{\mathrm{T}}^{\mathrm{min}})$:

$$(\sigma\mathcal{B}A\epsilon)_{\mathrm{excl}} = \frac{(\sigma\mathcal{B}A\epsilon)_{\mathrm{MI}}(m_{\mathrm{T}}^{\mathrm{min}})}{f_{m_{\mathrm{T}}}(m_{\mathrm{T}}^{\mathrm{min}})} \tag{5}$$

Here, $\mathcal{B}$ is the branching fraction of the new particle decaying to $\tau + \nu$. A new physics model can be interpreted using the MI limit by scanning $m_{\mathrm{T}}^{\mathrm{min}}$ for the minimum value of $(\sigma\mathcal{B}A\epsilon)_{\mathrm{excl}}$. When accounting for the model-dependent part of $A\epsilon$, $(\sigma\mathcal{B})_{\mathrm{excl}}$ can be extracted. Models with a theoretical cross section $(\sigma\mathcal{B})_{\mathrm{theo}} > (\sigma\mathcal{B})_{\mathrm{excl}}$ can be excluded. The procedure described here can be applied to all models involving the two-body decay of a massive system to a τ lepton and $p_{\mathrm{T}}^{\mathrm{miss}}$, which exhibit back-to-back kinematics similar to those of a generic W′ boson. If the kinematic properties are different, the fraction of events $f_{m_{\mathrm{T}}}(m_{\mathrm{T}}^{\mathrm{min}})$ must be determined for the particular model considered.

8.2 Mass limit for a heavy vector boson

When calculating the limit in the SSM, the parameter of interest is the product of the signal production cross section and the branching fraction $\sigma\mathcal{B}(\mathrm{W}' \to \tau\nu)$. Figure 6 shows the exclusion limit on this product as a function of the SSM $m_{\mathrm{W}'}$. The SSM W′ boson production is excluded for masses between 0.6 TeV and 4.8 TeV by comparison with the theoretical NNLO cross section. The observed limit is in agreement with the expected mass limit of 4.8 TeV. Previous CMS searches in this channel already exclude the lower SSM mass hypotheses [6]. The lower bound is mainly determined by the trigger thresholds and the upper bound by the available data. In the high mass region, off-shell production of W′ bosons becomes dominant, shifting the signal m_{T} distribution towards lower m_{T} values.

8.3 The NUGIM and coupling sensitivity

The limits for the coupling-dependent W′ boson model and the NUGIM G(221) model are calculated in a two-dimensional plane that depends on the mass of the new mediator particle and its width. The W′ boson width is affected by the coupling. We extract the limits shown in Fig. 7 by finding the intersection of the LO cross section theory plane of the corresponding model with the experimental result. The upper limits on the coupling strength in the case

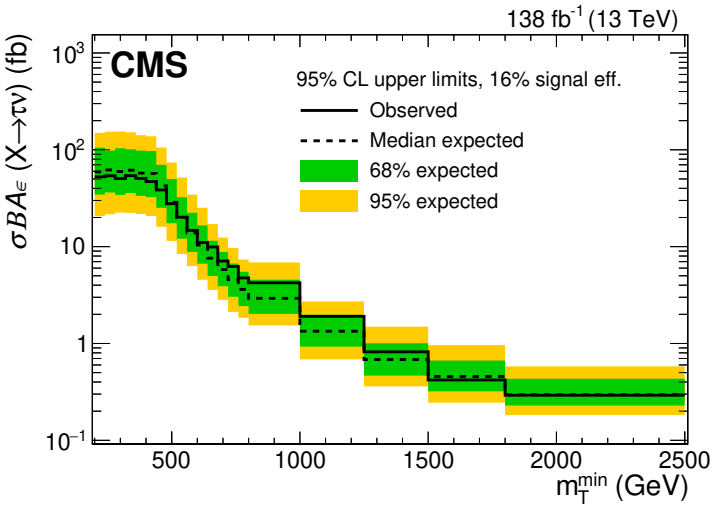

Figure 5: Bayesian 95% CL model-independent upper limit on the product of signal cross section and branching fraction for the τ +ν decay for a back-to-back τ lepton plus $p_{\mathrm{T}}^{\mathrm{miss}}$ topology. To calculate this limit, all events for signal, background, and data are summed starting from a minimum m_{T} threshold and then divided by the total number of events. No assumption on the signal shape is included in this limit, however a signal selection efficiency of 16% is assumed. The expected (dashed line) and observed (solid line) limits are shown as well as the 68% and 95% CL uncertainty bands (green and yellow, respectively). The uncertainty bands correspond to the sum in quadrature of PDF and scale variations.

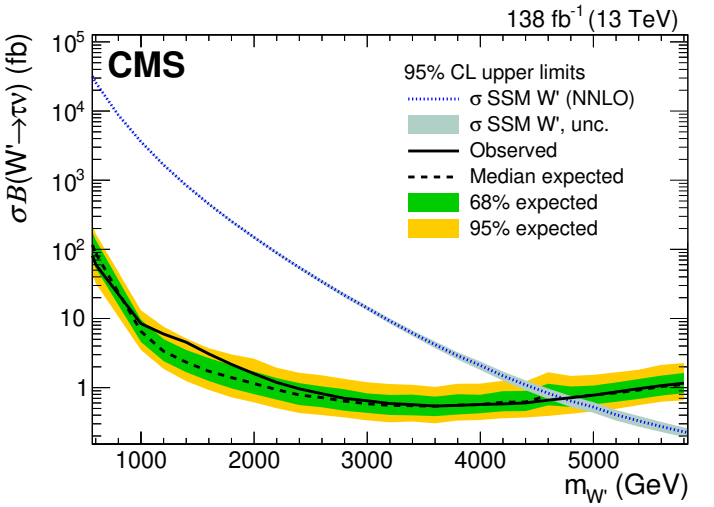

Figure 6: Bayesian upper exclusion limits at 95% CL on the product of the cross section and branching fraction of a W′ boson decaying to a τ lepton and a neutrino in the SSM model. For this model, W′ boson masses of up to 4.8 TeV can be excluded. The limit is given by the intersection of the observed (solid) limit and the theoretical cross section (blue dotted curve). The 68 and 95% quantiles of the limits are represented by the green and yellow bands, respectively. The $\sigma\mathcal{B}$ for an SSM W′ boson, along with its associated uncertainty, calculated at NNLO precision in QCD is shown.

of SSM-like W′ bosons, and on the mixing parameter $\cot\theta_E$ in the case of the NUGIM G(221) model are provided as functions of $m_{W'}$. In the latter case, for $\cot(\theta_E) > 5.5$, the width becomes so large that the model is no longer valid. We exclude coupling values above $g_{W'}/g_W = 0.05$ for masses of 1 TeV. For a mass hypothesis of 6 TeV, coupling values above 2 are excluded. For NUGIM G(221) models, we can exclude all theoretically allowed values of $\cot\theta_E$ for masses below 2.2 TeV. For values of $\cot\theta_E = 1$, masses of up to 4.8 TeV are excluded.

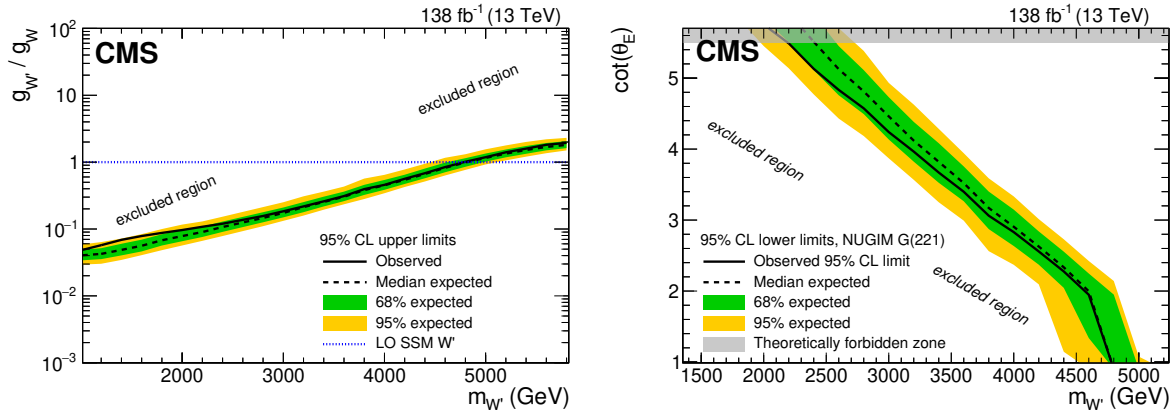

Figure 7: Bayesian upper exclusion limits on the ratio $g_{W'}/g_W$ for an SSM-like W′ boson are shown on the left. The unity coupling ratio (blue dotted curve) corresponds to the SSM common benchmark. The lower exclusion limits on the NUGIM G(221) mixing angle $\cot\theta_E$ are shown on the right as a function of the W′ boson mass. The theoretically excluded region is shaded in grey. The 68 and 95% quantiles of the limits are represented by the green and yellow bands, respectively.

8.4 The QBH limits

The QBH model has the same m_T sensitive observable as the SSM model. However, it differs with respect to its production mechanism. Its signal shape in the generator mass distribution is characterized by a threshold mass with a rising edge, followed by a monotonic decrease towards higher masses. This shape is less sharp in the m_T distribution and, in parts, extends towards lower masses because of the τ lepton decay. We exclude this model for threshold masses of up to 6.6 TeV, as shown in Fig. 8.

8.5 Leptoquark limits

We also place upper limits on the cross section of the process $pp \to \tau\nu$ mediated by LQ exchange in the t-channel. These limits are presented in Fig. 9. Masses up to 205/ 515 / 5900 GeV are excluded for the best-fit LH / best-fit LH+RH / democratic scenarios.

Figure 10 shows lower limits on the LQ mass for varying LQ couplings g_U to SM fermions. The limits are compared to the values of g_U that are obtained in the fit [44] to the flavor anomaly data in the two best fit scenarios for only LH couplings (left) and LH+RH couplings (right).

In both best-fit scenarios, we exclude a significant part of the LQ parameter space. LQ masses up to 10 TeV and couplings g_U of up to 8 are probed. In comparison to the values of g_U preferred to explain the flavor anomalies, this analysis has direct sensitivity to LQs, as predicted by the model of Ref. [44]. The exclusion limits at 95% CL just reach the preferred phase space at large values of m_{LQ} and g_U. In addition to exclusion limits probing the couplings as predicted in the best fit scenarios, limits that are not motivated by the b anomalies are presented as well. They

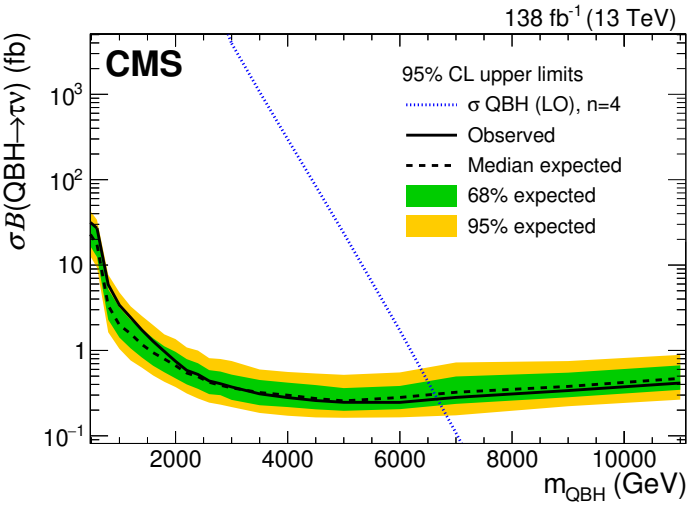

Figure 8: Bayesian upper exclusion limits at 95% CL on the product of the production cross section and branching fraction of a QBH in an associated τ lepton and neutrino final state. The 68 and 95% quantiles of the limits are represented by the green and yellow bands, respectively. Masses of up to 6.6 TeV are excluded at 95% CL. The limit is given by the intersection of the observed (solid) limit and the theoretical cross section (blue dotted curve).

are obtained using the benchmark of democratic LH couplings. The lower limits on m_{LQ} are shown for varying values of g_{U} in Fig. 10 (lower) for this scenario.

8.6 The EFT limits

In the EFT description, we calculate limits in terms of the three Wilson coefficients used in this model. For each available signal hypothesis, the event yield is scaled with the square of the corresponding Wilson coefficient to probe a range between 0.05 and 2.0 for each coupling type, and the direct limit on the maximum allowed coupling value is extracted. The results are shown in Fig. 11. The excluded values are 0.32 (0.27) / 0.51 (0.41) / 0.27 (0.22) observed (expected) for ϵ_{L} / ϵ_{SL} / ϵ_{T}, respectively. The small difference originates from the shape of the signals, for which the m_{T}-region between 1.0 and 1.5 TeV has the most impact on the exclusion limits [57].

8.7 Overview of the exclusion limits

A summary of mass exclusion limits calculated at 95% CL is shown in Table 1. The limits presented in this analysis are the most stringent to date for all the models considered.

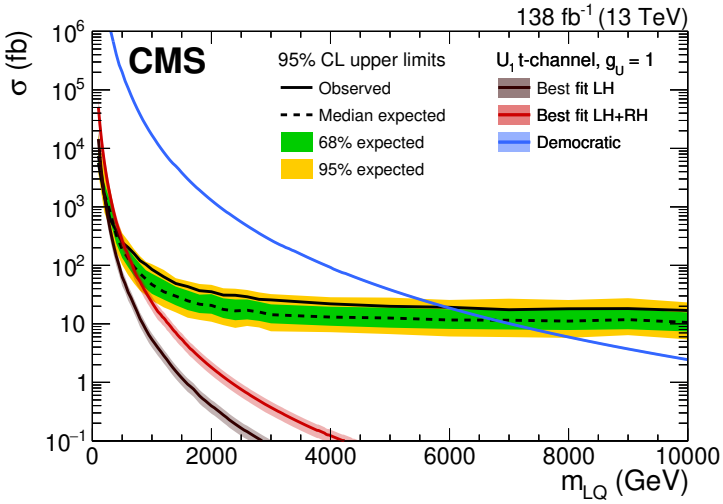

Figure 9: Bayesian upper limits at 95% CL on the cross section of the process $pp \to \tau\nu$ mediated by LQ exchange in the t-channel. The inner (green) band and the outer (yellow) band indicate the regions containing 68 and 95%, respectively, of the distribution of limits expected under the background-only hypothesis. The predicted LQ cross section at LO in the three coupling benchmark scenarios is depicted in different colors for $g_U = 1$. The uncertainty bands correspond to the sum in quadrature of PDF and scale variations. The first benchmark scenario considers only couplings to LH SM fermions (i.e. $\beta_R^{ij} = 0$) and is referred to as "best fit LH". The second benchmark, referred to as "best fit LH+RH", considers $\left|\beta_R^{b\tau}\right| = 1$ and all other $\beta_R^{ij} = 0$. In the third "democratic" benchmark, equal couplings only to LH fermions are assumed, i.e., $\left|\beta_L^{ij}\right| = 1$ and $\beta_R^{ij} = 0$ for all i and j.

Table 1: Summary of 95% CL exclusion limits (expected and observed) derived from 2016–2018 data, for the physics models studied in this analysis: sequential standard model (SSM), nonuniversal gauge interaction model (NUGIM), a quantum black hole (QBH) interpretation, t-channel leptoquark (LQ), and effective field interpretation (EFT).

Model	Parameter	Expected Limit	Observed Limit
SSM $W' \to \tau + \nu$	$m_{W'}$	4.8 TeV	4.8 TeV
NUGIM $\cot(\theta_E)$=1	$m_{W'}$	4.8 TeV	4.8 TeV
NUGIM $\cot(\theta_E)$=5.5	$m_{W'}$	2.4 TeV	2.2 TeV
QBH	m_{QBH}	6.6 TeV	6.6 TeV
LQ democratic, g_U=1.0	m_{LQ}	6.7 TeV	5.9 TeV
LQ best-fit LH, g_U=1.0	m_{LQ}	145 GeV	205 GeV
LQ best-fit LH, g_U=2.5	m_{LQ}	1.8 TeV	1.5 TeV
LQ best-fit LH+RH, g_U=1.0	m_{LQ}	645 GeV	515 GeV
LQ best-fit LH+RH, g_U=2.5	m_{LQ}	3.0 TeV	2.5 TeV
EFT	ϵ_L^{cb}	0.27	0.32
EFT	ϵ_{SL}^{cb}	0.41	0.51
EFT	ϵ_T^{cb}	0.22	0.27

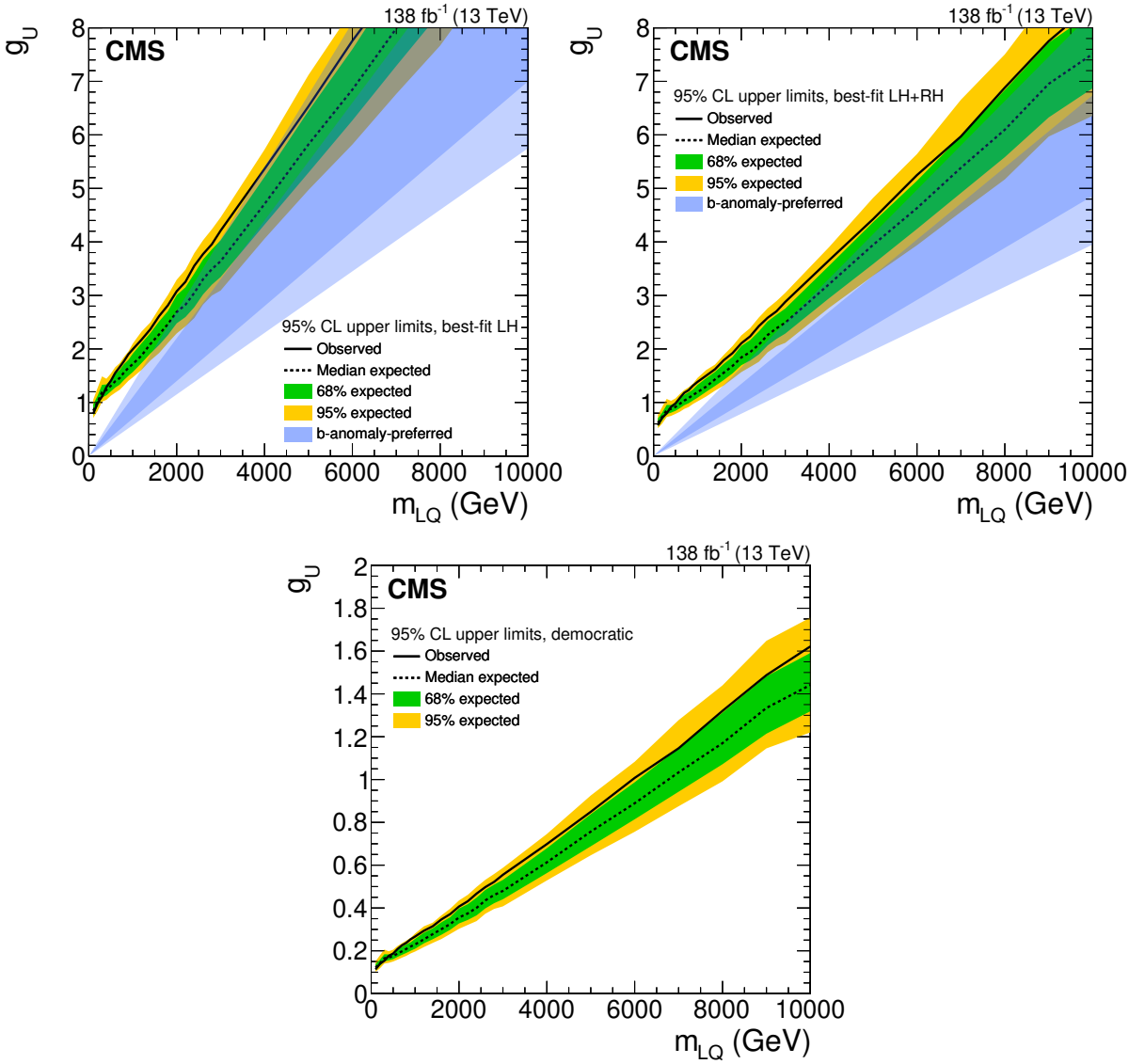

Figure 10: Expected and observed upper limits of the LQ coupling g_U as a function of the mass in the LH (left), LH+RH (right), and democratic (lower) scenarios. The blue band shows the 68 and 95% regions of g_U preferred by the fit to the b anomalies data [44].

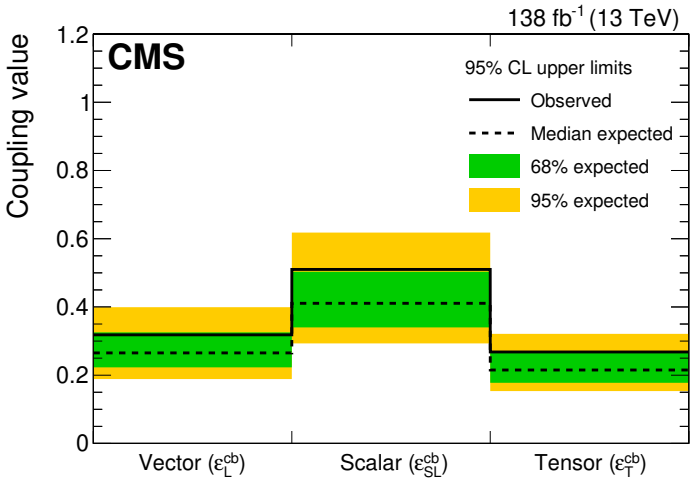

Figure 11: Bayesian upper exclusion limits at 95% CL on each of the Wilson coefficients described by the EFT model in Section 3 based on 2016–2018 data. The three different coupling types represent a LH vector coupling ($\epsilon_{\mathrm{L}}^{\mathrm{cb}}$), scalar-tensor-like coupling ($\epsilon_{\mathrm{S_L}}^{\mathrm{cb}}$, and tensor-like coupling ($\epsilon_{\mathrm{T}}^{\mathrm{cb}}$)). The 68 and 95% quantiles of the limits are represented by the green and yellow bands, respectively.

9 Summary

A search for new resonant phenomena in the transverse mass distribution of a hadronically decaying τ lepton and missing transverse momentum final state has been performed. The analysis uses 2016–2018 data collected with the CMS detector in proton-proton collisions with $\sqrt{s} = 13\,\text{TeV}$ at the LHC, corresponding to an integrated luminosity of 138 fb^{-1}. The newly developed DEEPTAU algorithm is used to identify τ lepton candidates and to separate signal from background. Background from jets being misidentified as hadronically decaying τ lepton candidates is derived from data.

No significant deviation from the standard model expectations is observed. Upper limits are set at 95% confidence level on the product of the production cross section and branching fraction $\sigma\mathcal{B}$ of a new resonance gauge boson (W') decaying to a τ lepton and a neutrino. Lower limits are derived on the mass of a W' boson in the sequential standard model and on the mass of a quantum black hole. In the case of the generalized coupling model, upper limits on $\sigma\mathcal{B}$ are translated into upper exclusion limits on the ratio of the couplings of the W' boson to that of the standard model W boson, $g_{\text{W}'}/g_{\text{W}}$. Similarly, limits are obtained on the mixing angle θ_E for the nonuniversal gauge interaction model and on the Wilson coefficients for an effective field theory model.

The process of t-channel leptoquark (LQ) exchange is targeted explicitly in this analysis. For the first time, upper limits are placed on the cross section of the $\text{pp} \to \tau\nu$ process mediated by t-channel LQ exchange. Three benchmark coupling scenarios are tested that correspond to the best fits to the flavor anomaly data and to a generic democratic flavor structure. Significant portions of the LQ parameter space are excluded by placing upper limits on the LQ coupling g_{U} as a function of the LQ mass, including parts of the region preferred by a vector LQ explanation of the anomalies. Additionally, a model-independent limit is provided. The limits obtained for the various interpretations presented are the most stringent to date.

References

[1] R. N. Mohapatra and J. C. Pati, "Natural left-right symmetry", *Phys. Rev. D* **11** (1975) 2558, doi:10.1103/PhysRevD.11.2558.

[2] R. N. Mohapatra and J. C. Pati, "Left-right gauge symmetry and an isoconjugate model of CP violation", *Phys. Rev. D* **11** (1975) 566, doi:10.1103/PhysRevD.11.566.

[3] ATLAS Collaboration, "Search for a heavy charged boson in events with a charged lepton and missing transverse momentum from pp collisions at $\sqrt{s} = 13\,\text{TeV}$ with the ATLAS detector", *Phys. Rev. D* **100** (2019) 052013, doi:10.1103/PhysRevD.100.052013, arXiv:1906.05609.

[4] CMS Collaboration, "Search for new physics in the lepton plus missing transverse momentum final state in proton-proton collisions at $\sqrt{s} = 13\,\text{TeV}$", *JHEP* **07** (2022) 067, doi:10.1007/JHEP07(2022)067, arXiv:2202.06075.

[5] G. Altarelli, B. Mele, and M. Ruiz-Altaba, "Searching for new heavy vector bosons in $\text{p}\overline{\text{p}}$ colliders", *Z. Phys. C* **45** (1989) 109, doi:10.1007/BF01552335. [Erratum: doi:10.1007/BF01556677].

[6] CMS Collaboration, "Search for W′ decaying to tau lepton and neutrino in proton-proton collisions at $\sqrt{s} = 8\,\text{TeV}$", *Phys. Lett. B* **755** (2016) 196, doi:10.1016/j.physletb.2016.02.002, arXiv:1508.04308.

[7] CMS Collaboration, "Search for a W′ boson decaying to a τ lepton and a neutrino in proton-proton collisions at $\sqrt{s} = 13\,\text{TeV}$", *Phys. Lett. B* **792** (2019) 107, doi:10.1016/j.physletb.2019.01.069, arXiv:1807.11421.

[8] ATLAS Collaboration, "Search for high-mass resonances decaying to $\tau\nu$ in pp collisions at $\sqrt{s} = 13\,\text{TeV}$ with the ATLAS detector", *Phys. Rev. Lett.* **120** (2018) 161802, doi:10.1103/PhysRevLett.120.161802, arXiv:1801.06992.

[9] BaBar Collaboration, "Evidence for an excess of $\bar{B} \to D^{(*)}\tau^-\bar{\nu}_\tau$ decays", *Phys. Rev. Lett.* **109** (2012) 101802, doi:10.1103/PhysRevLett.109.101802, arXiv:1205.5442.

[10] BaBar Collaboration, "Measurement of an excess of $\bar{B} \to D^{(*)}\tau^-\bar{\nu}_\tau$ decays and implications for charged higgs bosons", *Phys. Rev. D* **88** (2013) 072012, doi:10.1103/PhysRevD.88.072012, arXiv:1303.0571.

[11] Belle Collaboration, "Measurement of the branching ratio of $\bar{B} \to D^{(*)}\tau^-\bar{\nu}_\tau$ relative to $\bar{B} \to D^{(*)}\ell^-\bar{\nu}_\ell$ decays with hadronic tagging at Belle", *Phys. Rev. D* **92** (2015) 072014, doi:10.1103/PhysRevD.92.072014, arXiv:1507.03233.

[12] Belle Collaboration, "Measurement of the τ lepton polarization and $R(D^*)$ in the decay $\bar{B} \to D^*\tau^-\bar{\nu}_\tau$", *Phys. Rev. Lett.* **118** (2017) 211801, doi:10.1103/PhysRevLett.118.211801, arXiv:1612.00529.

[13] Belle Collaboration, "Measurement of the τ lepton polarization and $R(D^*)$ in the decay $\bar{B} \to D^*\tau^-\bar{\nu}_\tau$ with one-prong hadronic τ decays at Belle", *Phys. Rev. D* **97** (2018) 012004, doi:10.1103/PhysRevD.97.012004, arXiv:1709.00129.

[14] Belle Collaboration, "Measurement of $\mathcal{R}(D)$ and $\mathcal{R}(D^*)$ with a semileptonic tagging method", *Phys. Rev. Lett.* **124** (2020) 161803, doi:10.1103/PhysRevLett.124.161803, arXiv:1910.05864.

[15] LHCb Collaboration, "Measurement of the ratio of branching fractions $\mathcal{B}(\bar{B}^0 \to D^{*+}\tau^-\bar{\nu}_\tau)/\mathcal{B}(\bar{B}^0 \to D^{*+}\mu^-\bar{\nu}_\mu)$", *Phys. Rev. Lett.* **115** (2015) 111803, doi:10.1103/PhysRevLett.115.111803, arXiv:1506.08614. [Erratum: *Phys. Rev. Lett.* **115** (2015) 159901].

[16] LHCb Collaboration, "Measurement of the ratio of the $B^0 \to D^{*-}\tau^+\nu_\tau$ and $B^0 \to D^{*-}\mu^+\nu_\mu$ branching fractions using three-prong τ-lepton decays", *Phys. Rev. Lett.* **120** (2018) 171802, doi:10.1103/PhysRevLett.120.171802, arXiv:1708.08856.

[17] LHCb Collaboration, "Test of lepton flavor universality by the measurement of the $B^0 \to D^{*-}\tau^+\nu_\tau$ branching fraction using three-prong τ decays", *Phys. Rev. D* **97** (2018) 072013, doi:10.1103/PhysRevD.97.072013, arXiv:1711.02505.

[18] LHCb Collaboration, "Search for lepton-universality violation in $B^+ \to K^+\ell^+\ell^-$ decays", *Phys. Rev. Lett.* **122** (2019) 191801, doi:10.1103/PhysRevLett.122.191801, arXiv:1903.09252.

[19] LHCb Collaboration, "Test of lepton universality with $B^0 \to K^{*0}\ell^+\ell^-$ decays", *JHEP* **08** (2017) 055, doi:10.1007/JHEP08(2017)055, arXiv:1705.05802.

[20] LHCb Collaboration, "Test of lepton universality in beauty-quark decays", *Nature Phys.* **18** (2022) 277, doi:10.1038/s41567-021-01478-8, arXiv:2103.11769.

[21] LHCb Collaboration, "Tests of lepton universality using $B^0 \to K^0_S \ell^+ \ell^-$ and $B^+ \to K^{*+} \ell^+ \ell^-$ decays", *Phys. Rev. Lett.* **128** (2022) 191802, doi:10.1103/PhysRevLett.128.191802, arXiv:2110.09501.

[22] M. Tanaka and R. Watanabe, "New physics in the weak interaction of $\bar{B} \to D^{(*)} \tau \bar{\nu}$", *Phys. Rev. D* **87** (2013) 034028, doi:10.1103/PhysRevD.87.034028, arXiv:1212.1878.

[23] Y. Sakaki, M. Tanaka, A. Tayduganov, and R. Watanabe, "Testing leptoquark models in $\bar{B} \to D^{(*)} \tau \bar{\nu}$", *Phys. Rev. D* **88** (2013) 094012, doi:10.1103/PhysRevD.88.094012, arXiv:1309.0301.

[24] I. Doršner, S. Fajfer, N. Košnik, and I. Nišandžić, "Minimally flavored colored scalar in $\bar{B} \to D^{(*)} \tau \bar{\nu}$ and the mass matrices constraints", *JHEP* **11** (2013) 084, doi:10.1007/JHEP11(2013)084, arXiv:1306.6493.

[25] B. Dumont, K. Nishiwaki, and R. Watanabe, "LHC constraints and prospects for S_1 scalar leptoquark explaining the $\bar{B} \to D^{(*)} \tau \bar{\nu}$ anomaly", *Phys. Rev. D* **94** (2016) 034001, doi:10.1103/PhysRevD.94.034001, arXiv:1603.05248.

[26] I. Doršner, S. Fajfer, D. A. Faroughy, and N. Košnik, "The role of the S_3 GUT leptoquark in flavor universality and collider searches", *JHEP* **10** (2017) 188, doi:10.1007/JHEP10(2017)188, arXiv:1706.07779.

[27] D. Bečirević et al., "Scalar leptoquarks from grand unified theories to accommodate the b-physics anomalies", *Phys. Rev. D* **98** (2018) 055003, doi:10.1103/PhysRevD.98.055003, arXiv:1806.05689.

[28] A. Crivellin, D. Müller, and T. Ota, "Simultaneous explanation of $R(D^{(*)})$ and $b \to s \mu^+ \mu^-$: the last scalar leptoquarks standing", *JHEP* **09** (2017) 040, doi:10.1007/JHEP09(2017)040, arXiv:1703.09226.

[29] B. Gripaios, M. Nardecchia, and S. A. Renner, "Composite leptoquarks and anomalies in b-meson decays", *JHEP* **05** (2015) 006, doi:10.1007/JHEP05(2015)006, arXiv:1412.1791.

[30] M. Bauer and M. Neubert, "Minimal leptoquark explanation for the $R_{D^{(*)}}$, R_K , and $(g-2)_\mu$ anomalies", *Phys. Rev. Lett.* **116** (2016) 141802, doi:10.1103/PhysRevLett.116.141802, arXiv:1511.01900.

[31] E. Coluccio Leskow, G. DAmbrosio, A. Crivellin, and D. Müller, "$(g-2)_\mu$, lepton flavor violation, and Z decays with leptoquarks: Correlations and future prospects", *Phys. Rev. D* **95** (2017) 055018, doi:10.1103/PhysRevD.95.055018, arXiv:1612.06858.

[32] D. Bečirević and O. Sumensari, "A leptoquark model to accommodate $R_K^{\rm exp} < R_K^{\rm SM}$ and $R_{K^*}^{\rm exp} < R_{K^*}^{\rm SM}$", *JHEP* **08** (2017) 104, doi:10.1007/JHEP08(2017)104, arXiv:1704.05835.

[33] G. Hiller and I. Nišandžić, "R_K and R_{K^*} beyond the standard model", *Phys. Rev. D* **96** (2017) 035003, doi:10.1103/PhysRevD.96.035003, arXiv:1704.05444.

[34] G. Hiller, D. Loose, and I. Nišandžić, "Flavorful leptoquarks at hadron colliders", *Phys. Rev. D* **97** (2018) 075004, doi:10.1103/PhysRevD.97.075004, arXiv:1801.09399.

[35] L. Di Luzio, A. Greljo, and M. Nardecchia, "Gauge leptoquark as the origin of B-physics anomalies", *Phys. Rev. D* **96** (2017) 115011, doi:10.1103/PhysRevD.96.115011, arXiv:1708.08450.

[36] L. Di Luzio et al., "Maximal flavour violation: a cabibbo mechanism for leptoquarks", *JHEP* **11** (2018) 081, doi:10.1007/JHEP11(2018)081, arXiv:1808.00942.

[37] L. Calibbi, A. Crivellin, and T. Li, "Model of vector leptoquarks in view of the *b*-physics anomalies", *Phys. Rev. D* **98** (2018) 115002, doi:10.1103/PhysRevD.98.115002, arXiv:1709.00692.

[38] M. Bordone, C. Cornella, J. Fuentes-Martin, and G. Isidori, "A three-site gauge model for flavor hierarchies and flavor anomalies", *Phys. Lett. B* **779** (2018) 317, doi:10.1016/j.physletb.2018.02.011, arXiv:1712.01368.

[39] R. Barbieri and A. Tesi, "*b*-decay anomalies in Pati-Salam SU(4)", *Eur. Phys. J. C* **78** (2018) 193, doi:10.1140/epjc/s10052-018-5680-9, arXiv:1712.06844.

[40] D. Buttazzo, A. Greljo, G. Isidori, and D. Marzocca, "B-physics anomalies: a guide to combined explanations", *JHEP* **11** (2017) 044, doi:10.1007/JHEP11(2017)044, arXiv:1706.07808.

[41] D. Marzocca, "Addressing the b-physics anomalies in a fundamental composite higgs model", *JHEP* **07** (2018) 121, doi:10.1007/JHEP07(2018)121, arXiv:1803.10972.

[42] M. J. Baker, J. Fuentes-Martin, G. Isidori, and M. König, "High-p_{T} signatures in vector–leptoquark models", *Eur. Phys. J. C* **79** (2019) 334, doi:10.1140/epjc/s10052-019-6853-x, arXiv:1901.10480.

[43] C. Cornella, J. Fuentes-Martin, and G. Isidori, "Revisiting the vector leptoquark explanation of the b-physics anomalies", *JHEP* **07** (2019) 168, doi:10.1007/JHEP07(2019)168, arXiv:1903.11517.

[44] C. Cornella et al., "Reading the footprints of the b-meson flavor anomalies", *JHEP* **08** (2021) 050, doi:10.1007/JHEP08(2021)050, arXiv:2103.16558.

[45] CMS Collaboration, "Constraints on models of scalar and vector leptoquarks decaying to a quark and a neutrino at $\sqrt{s} = 13\,\mathrm{TeV}$", *Phys. Rev. D* **98** (2018) 032005, doi:10.1103/PhysRevD.98.032005, arXiv:1805.10228.

[46] ATLAS Collaboration, "Search for a scalar partner of the top quark in the all-hadronic $t\bar{t}$ plus missing transverse momentum final state at $\sqrt{s} = 13\,\mathrm{TeV}$ with the ATLAS detector", *Eur. Phys. J. C* **80** (2020) 737, doi:10.1140/epjc/s10052-020-8102-8, arXiv:2004.14060.

[47] ATLAS Collaboration, "Search for new phenomena in final states with *b*-jets and missing transverse momentum in $\sqrt{s} = 13\,\mathrm{TeV}$ pp collisions with the ATLAS detector", *JHEP* **05** (2021) 093, doi:10.1007/JHEP05(2021)093, arXiv:2101.12527.

[48] CMS Collaboration, "Search for singly and pair-produced leptoquarks coupling to third-generation fermions in proton-proton collisions at $\sqrt{s} = 13\,\mathrm{TeV}$", *Phys. Lett. B* **819** (2021) 136446, doi:10.1016/j.physletb.2021.136446, arXiv:2012.04178.

[49] ATLAS Collaboration, "Search for pair production of scalar leptoquarks decaying into first- or second-generation leptons and top quarks in proton–proton collisions at $\sqrt{s} = 13$ TeV with the ATLAS detector", *Eur. Phys. J. C* **81** (2021) 313, doi:10.1140/epjc/s10052-021-09009-8, arXiv:2010.02098.

[50] CMS Collaboration, "Search for leptoquarks coupled to third-generation quarks in proton-proton collisions at $\sqrt{s} = 13$ TeV", *Phys. Rev. Lett.* **121** (2018) 241802, doi:10.1103/PhysRevLett.121.241802, arXiv:1809.05558.

[51] ATLAS Collaboration, "Search for pair production of third-generation scalar leptoquarks decaying into a top quark and a τ-lepton in pp collisions at $\sqrt{s}$ = 13 TeV with the ATLAS detector", *JHEP* **06** (2021) 179, doi:10.1007/JHEP06(2021)179, arXiv:2101.11582.

[52] CMS Collaboration, "Search for third-generation scalar leptoquarks decaying to a top quark and a τ lepton at $\sqrt{s} = 13$ TeV", *Eur. Phys. J. C* **78** (2018) 707, doi:10.1140/epjc/s10052-018-6143-z, arXiv:1803.02864.

[53] ATLAS Collaboration, "Search for new phenomena in pp collisions in final states with tau leptons, b-jets, and missing transverse momentum with the ATLAS detector", *Phys. Rev. D* **104** (2021) 112005, doi:10.1103/PhysRevD.104.112005, arXiv:2108.07665.

[54] CMS Collaboration, "Search for heavy neutrinos and third-generation leptoquarks in hadronic states of two τ leptons and two jets in proton-proton collisions at $\sqrt{s} = 13$ TeV", *JHEP* **03** (2019) 170, doi:10.1007/JHEP03(2019)170, arXiv:1811.00806.

[55] CMS Collaboration, "Search for a singly produced third-generation scalar leptoquark decaying to a τ lepton and a bottom quark in proton-proton collisions at $\sqrt{s} = 13$ TeV", *JHEP* **07** (2018) 115, doi:10.1007/JHEP07(2018)115, arXiv:1806.03472.

[56] L. Di Luzio and M. Nardecchia, "What is the scale of new physics behind the B-flavour anomalies?", *Eur. Phys. J. C* **77** (2017) 536, doi:10.1140/epjc/s10052-017-5118-9, arXiv:1706.01868.

[57] A. Greljo, J. Martin Camalich, and J. D. Ruiz-'Alvarez, "Mono-τ signatures at the LHC constrain explanations of b-decay anomalies", *Phys. Rev. Lett.* **122** (2019) 131803, doi:10.1103/PhysRevLett.122.131803, arXiv:1811.07920.

[58] S. Dimopoulos and G. L. Landsberg, "Black holes at the LHC", *Phys. Rev. Lett.* **87** (2001) 161602, doi:10.1103/PhysRevLett.87.161602, arXiv:hep-ph/0106295.

[59] S. B. Giddings and S. D. Thomas, "High-energy colliders as black hole factories: The end of short distance physics", *Phys. Rev. D* **65** (2002) 056010, doi:10.1103/PhysRevD.65.056010, arXiv:hep-ph/0106219.

[60] P. Meade and L. Randall, "Black holes and quantum gravity at the LHC", *JHEP* **05** (2008) 003, doi:10.1088/1126-6708/2008/05/003, arXiv:0708.3017.

[61] HEPData record for this analysis, 2022. doi:10.17182/hepdata.135472.

[62] CMS Collaboration, "Performance of the CMS level-1 trigger in proton-proton collisions at $\sqrt{s} = 13$ TeV", *JINST* **15** (2020) P10017, doi:10.1088/1748-0221/15/10/P10017, arXiv:2006.10165.

[63] CMS Collaboration, "The CMS trigger system", *JINST* **12** (2017) P01020, doi:10.1088/1748-0221/12/01/P01020, arXiv:1609.02366.

[64] CMS Collaboration, "The CMS experiment at the CERN LHC", *JINST* **3** (2008) S08004, doi:10.1088/1748-0221/3/08/S08004.

[65] C.-W. Chiang, N. G. Deshpande, X.-G. He, and J. Jiang, "The family $SU(2)_l \times SU(2)_h \times U(1)$ model", *Phys. Rev. D* **81** (2010) 015006, doi:10.1103/PhysRevD.81.015006, arXiv:0911.1480.

[66] Y. G. Kim and K. Y. Lee, "Early LHC bound on the W′ boson mass in the nonuniversal gauge interaction model", *Phys. Lett. B* **706** (2012) 367, doi:10.1016/j.physletb.2011.11.032, arXiv:1105.2653.

[67] L. Edelhauser and A. Knochel, "Observing nonstandard W′ and Z′ through the third generation and Higgs lens", 2014. arXiv:1408.0914.

[68] N. Arkani-Hamed, S. Dimopoulos, and G. Dvali, "The hierarchy problem and new dimensions at a millimeter", *Phys. Lett. B* **429** (1998) 263, doi:10.1016/s0370-2693(98)00466-3.

[69] W. Buchmüller, R. Rückl, and D. Wyler, "Leptoquarks in lepton - quark collisions", *Phys. Lett. B* **191** (1987) 442, doi:10.1016/S0370-2693(99)00014-3. [Erratum: *Phys. Lett. B* 448 (1999) 320].

[70] S. Agostinelli et al., "GEANT4—a simulation toolkit", *Nucl. Instrum. Meth. A* **506** (2003) 250, doi:10.1016/S0168-9002(03)01368-8.

[71] CMS Collaboration, "Precision luminosity measurement in proton-proton collisions at $\sqrt{s} = 13$ TeV in 2015 and 2016 at CMS", *Eur. Phys. J. C* **81** (2021) 800, doi:10.1140/epjc/s10052-021-09538-2, arXiv:2104.01927.

[72] CMS Collaboration, "CMS luminosity measurement for the 2017 data-taking period at $\sqrt{s} = 13$ TeV", CMS Physics Analysis Summary CMS-PAS-LUM-17-004, 2018.

[73] CMS Collaboration, "CMS luminosity measurement for the 2018 data-taking period at $\sqrt{s} = 13$ TeV", CMS Physics Analysis Summary CMS-PAS-LUM-18-002, 2019.

[74] P. Skands, S. Carrazza, and J. Rojo, "Tuning PYTHIA 8.1: the monash 2013 tune", *Eur. Phys. J. C* **74** (2014) 3024, doi:10.1140/epjc/s10052-014-3024-y, arXiv:1404.5630.

[75] CMS Collaboration, "Extraction and validation of a new set of CMS PYTHIA8 tunes from underlying-event measurements", *Eur. Phys. J. C* **80** (2020) 4, doi:10.1140/epjc/s10052-019-7499-4, arXiv:1903.12179.

[76] T. Sjöstrand et al., "An introduction to PYTHIA 8.2", *Comp. Phys. Comm.* **191** (2015) 159, doi:10.1016/j.cpc.2015.01.024, arXiv:1410.3012.

[77] R. D. Ball et al., "Parton distributions with LHC data", *Nucl. Phys. B* **867** (2013) 244, doi:10.1016/j.nuclphysb.2012.10.003, arXiv:1207.1303.

[78] NNPDF Collaboration, "Parton distributions from high-precision collider data", *Eur. Phys. J. C* **77** (2017) 663, doi:10.1140/epjc/s10052-017-5199-5, arXiv:1706.00428.

[79] J. Alwall et al., "Madgraph 5: going beyond", *JHEP* **06** (2011) 128, doi:10.1007/JHEP06(2011)128, arXiv:1106.0522.

[80] J. Alwall et al., "The automated computation of tree-level and next-to-leading order differential cross sections, and their matching to parton shower simulations", *JHEP* **07** (2014) 079, doi:10.1007/JHEP07(2014)079, arXiv:1405.0301.

[81] CMS Collaboration, "Search for a third-generation leptoquark coupling to a τ lepton and a b quark through single, pair and nonresonant production at $\sqrt{s} = 13$ TeV", CMS Physics Analysis Summary CMS-PAS-EXO-19-016, 2022.

[82] D. M. Gingrich, "Quantum black holes with charge, colour, and spin at the LHC", *J. Phys. G* **37** (2010) 105008, doi:10.1088/0954-3899/37/10/105008, arXiv:0912.0826.

[83] J. Pumplin et al., "New generation of parton distributions with uncertainties from global QCD analysis", *JHEP* **07** (2002) 012, doi:10.1088/1126-6708/2002/07/012, arXiv:hep-ph/0201195.

[84] R. Alonso, A. Kobach, and J. Martin Camalich, "New physics in the kinematic distributions of $\bar{B} \to D^{(*)}\tau^-(\to \ell^-\bar{\nu}_\ell\nu_\tau)\bar{\nu}_\tau$", *Phys. Rev. D* **94** (2016) 094021, doi:10.1103/PhysRevD.94.094021, arXiv:1602.07671.

[85] P. Nason, "A new method for combining NLO QCD with shower monte carlo algorithms", *JHEP* **11** (2004) 040, doi:10.1088/1126-6708/2004/11/040, arXiv:hep-ph/0409146.

[86] S. Frixione, P. Nason, and C. Oleari, "Matching NLO QCD computations with parton shower simulations: the POWHEG method", *JHEP* **11** (2007) 070, doi:10.1088/1126-6708/2007/11/070, arXiv:0709.2092.

[87] S. Alioli, P. Nason, C. Oleari, and E. Re, "A general framework for implementing NLO calculations in shower monte carlo programs: the POWHEG BOX", *JHEP* **06** (2010) 043, doi:10.1007/JHEP06(2010)043, arXiv:1002.2581.

[88] A. Buckley et al., "LHAPDF6: parton density access in the LHC precision era", *Eur. Phys. J. C* **75** (2015) 132, doi:10.1140/epjc/s10052-015-3318-8, arXiv:1412.7420.

[89] G. Balossini et al., "Combination of electroweak and QCD corrections to single W production at the Fermilab Tevatron and the CERN LHC", *JHEP* **01** (2010) 013, doi:10.1007/JHEP01(2010)013, arXiv:0907.0276.

[90] J. R. Andersen et al., "Les Houches 2013: Physics at TeV colliders: Standard model working group report", 2014. arXiv:1405.1067.

[91] A. Arbuzov et al., "Update of the MCSANC monte carlo integrator, v. 1.20", *JETP Lett.* **103** (2016) 131, doi:10.1134/S0021364016020041, arXiv:1509.03052.

[92] S. G. Bondarenko and A. A. Sapronov, "NLO EW and QCD proton-proton cross section calculations with mcsanc-v1.01", *Comput. Phys. Commun.* **184** (2013) 2343, doi:10.1016/j.cpc.2013.05.010, arXiv:1301.3687.

[93] CMS Collaboration, "Particle-flow reconstruction and global event description with the CMS detector", *JINST* **12** (2017) P10003, doi:10.1088/1748-0221/12/10/P10003, arXiv:1706.04965.

[94] M. Cacciari, G. P. Salam, and G. Soyez, "The anti-k_{T} jet clustering algorithm", *JHEP* **04** (2008) 063, doi:10.1088/1126-6708/2008/04/063, arXiv:0802.1189.

[95] M. Cacciari, G. P. Salam, and G. Soyez, "Fastjet user manual", *Eur. Phys. J. C* **72** (2012) 1896, doi:10.1140/epjc/s10052-012-1896-2, arXiv:1111.6097.

[96] CMS Collaboration, "Jet energy scale and resolution in the CMS experiment in pp collisions at 8 tev", *JINST* **12** (2017) P02014, doi:10.1088/1748-0221/12/02/P02014, arXiv:1607.03663.

[97] CMS Collaboration, "Performance of missing transverse momentum reconstruction in proton-proton collisions at $\sqrt{s} = 13\,\text{TeV}$ using the CMS detector", *JINST* **14** (2019) P07004, doi:10.1088/1748-0221/14/07/P07004, arXiv:1903.06078.

[98] CMS Collaboration, "Reconstruction and identification of τ lepton decays to hadrons and ν_τ at CMS", *JINST* **11** (2016) P01019, doi:10.1088/1748-0221/11/01/P01019, arXiv:1510.07488.

[99] CMS Collaboration, "Identification of hadronic tau lepton decays using a deep neural network", *JINST* **17** (2022) P07023, doi:10.1088/1748-0221/17/07/P07023, arXiv:2201.08458.

[100] CMS Collaboration, "Electron and photon reconstruction and identification with the CMS experiment at the CERN LHC", *JINST* **16** (2021) P05014, doi:10.1088/1748-0221/16/05/P05014, arXiv:2012.06888.

[101] CMS Collaboration, "Performance of the CMS muon detector and muon reconstruction with proton-proton collisions at $\sqrt{s} = 13\,\text{TeV}$", *JINST* **13** (2018) P06015, doi:10.1088/1748-0221/13/06/P06015, arXiv:1804.04528.

[102] J. Butterworth et al., "PDF4LHC recommendations for LHC Run II", *J. Phys. G* **43** (2016) 023001, doi:10.1088/0954-3899/43/2/023001, arXiv:1510.03865.

[103] CMS Collaboration, "Measurement of the inelastic proton-proton cross section at $\sqrt{s} = 13\,\text{TeV}$", *JHEP* **07** (2018) 161, doi:10.1007/JHEP07(2018)161, arXiv:1802.02613.

[104] R. Barlow and C. Beeston, "Fitting using finite monte carlo samples", *Computer Physics Communications* **77** (1993) 219, doi:10.1016/0010-4655(93)90005-W.

[105] Particle Data Group, "Review of particle physics", *Prog. Theor. Exp. Phys.* **2020** (2020) O83C01, doi:10.1093/ptep/ptaa104.

[106] The ATLAS Collaboration, The CMS Collaboration, and the LHC Higgs Combination Group, "Procedure for the LHC Higgs boson search combination in Summer 2011", Technical Report CMS-NOTE-2011-005, ATL-PHYS-PUB-2011-11, 2011.

[107] L. Moneta et al., "The RooStats project", in *13th International Workshop on Advanced Computing and Analysis Techniques in Physics Research (ACAT2010)*. SISSA, 2010. arXiv:1009.1003. PoS(ACAT2010)057. doi:10.22323/1.093.0057.